Electronic Supplementary Information

Experimental Section

Materials.

Iron (III) nitrate nonahydrate ($Fe(NO_3)_3 \cdot 9H_2O$), urea (CH_4N_2O), potassium hydroxide (KOH), sodium carbonate (Na_2CO_3), Nafion (5 wt.%), tetramethylammonium hydroxide (TMAOH), phosphoric acid (H_3PO_4), N,N-diethyl-p-phenylenediami (DPD), ammonium fluoride (NH_4F), ethylenediaminetetraacetic acid disodium (EDTA-2Na), and sodium hydroxide (NaOH) were purchased from Shanghai Maclin Biochemical Technology Co., Ltd. Nickel nitrate hexahydrate ($Ni(NO_3)_2 \cdot 6H_2O$), sulfuric acid (H_2SO_4), ethanol (C_2H_5OH), potassium permanganate ($KMnO_4$), and hydrochloric acid (HCl) were purchased from Beijing Chemical Reagent Co., Ltd (Beijing, China). Poly(3,4-ethylenedioxythiophene) polystyrene sulfonate (PEDOT:PSS) was bought from Shanghai Titan Scientific Co., Ltd. (Shanghai, China), ruthenium oxide (RuO_2), and Lithium perchlorate ($LiClO_4$) were obtained from Aladdin (Shanghai, China). Ni foam (NF) was purchased from Shenzhen Green and Creative Environmental Science and Technology Co., Ltd. Natural seawater was collected from Qingdao, Shandong, China. Prior to use, 3.4 g of Na_2CO_3 was added to 500 mL of seawater to precipitate magnesium and calcium salts. After filtration, 29.5 g of KOH was added, and any resulting precipitate was removed similarly to yield alkaline seawater.

Synthesis of NiFe LDH/NF and NiFe LDH@PP/NF.

Firstly, a piece of NF ($2.0 \times 3.0\ cm^2$) underwent sonication sequentially in 3 M HCl, ethanol, and ultrapure water, at least for 15 min for each step. The pretreated NF was then immersed in a solution composition $Ni(NO_3)_2 \cdot 6H_2O$ (1 mmol), $Fe(NO_3)_3 \cdot 9H_2O$ (1 mmol), $CO(NH_2)_2$ (10 mmol), NH_4F (4 mmol), and Ultrapure water (30 mL) within a Teflon-lined autoclave. Subsequently, the autoclave was heated at 120 °C for 6 h to obtain NiFe LDH/NF. NiFe LDH@PP/NF was prepared by immersing NiFe LDH/NF in an ultrapure water-based solution containing commercial PEDOT:PSS for 2 min (with loading mass of $0.4\ mg\ cm^{-2}$).

Preparation for RuO_2/NF.

5 mg RuO_2 was added into a solution containing 30 μL of Nafion, 485 μL of ethanol, and 485 μL of deionized water with the aid of ultrasonication (30 min) to form a homogeneous ink (5 mg mL^{-1}). 300 μL of catalyst ink was dropped onto a piece of cleaned NF ($0.5 \times 0.5\ cm^2$) with a loading mass of 6 mg cm^{-2}.

Characterization.

X-ray diffraction (XRD) studies the crystal structure of materials using a Philip D8 diffractometer and a Cu Ka radiation source. Scanning electron microscopy (SEM) images were collected on a Gemini SEM 300 scanning electron microscope (ZEISS, Germany) at an accelerating voltage of 5 kV. Transmission electron microscopy (TEM) images were acquired on a Jem-2100F electron microscope operated at 200 kV. X-ray photoelectron spectroscopy (XPS) measurements were performed on an ESCALAB 250 Xi Quantitative Scanning Microprobe. Ultraviolet-visible (UV-vis) spectrophotometry (Shimadzu UV-2700) was utilized for absorbance measurements. Raman spectroscopy was recorded on the LabRAM HR Evolution confocal microscope with a source length of 532 nm. Fourier transform infrared (FT-IR) spectra were collected on the Nexus 670.

Electrochemical measurements.

Electrochemical OER experiments were performed with the CHI660E electrochemical workstation, using the prepared samples ($0.5 \times 0.5\ cm^2$), carbon rod, and Hg/HgO as the working electrode, counter electrode, and reference electrode, respectively. Linear scanning voltammetry (LSV) curves were recorded in the range of 0 to 1.3 V at a scan rate of 5 mV^{-1}, and the scan mode of OER is back sweep. The pH values of 1 M KOH + seawater is approximately 14. Electrochemical impedance spectroscopy tests were conducted across a frequency range from 2×10^5 to 0.01 Hz with an amplitude of 1 mV in 1 M KOH + seawater. All measured potentials were referenced to that of RHE ($E_{RHE} = E_{Hg/HgO} + 0.098 + 0.059 \times pH$). The iR-compensated potential was obtained after the correction of solution resistance measured following the equation: $E_{corr} = E - iR$, where E is the original potential, R is the solution resistance, i is the corresponding current, and E_{corr} is the 100% iR-compensated potential. All data have been reported with iR compensation (except Fig. 3a, 3b, S5, and S13).

Detection of active chlorine.

The concentration of active chlorine in the electrolyte was determined based on the DPD method using a UV-vis spectrophotometer. Firstly, the 100 μL of electrolyte was successively mixed with 50 μL of H_2SO_4 (1.0 M), 50 μL of NaOH (2.0 M), and 4.8 mL of deionized water. Then, 250 μL of DPD reagent and 250 μL of PBS (pH = 6.5) were added to the above solution. After two minutes, the color of the solution changed to transparent pink. The absorbance at 550 nm was measured by UV-visible absorption spectroscopy, and the concentration of different active chlorine were also analyzed.

Energy efficiency and cost assessment.

Electrolyzer power = 2.4 V × 0.5 A cm^{-2} = 1.2 W cm^{-2}. The lower heating value (LHV) of H_2 is applied to calculate the efficiencies of NiFe LDH@PP/NF electrocatalyst. LHV = 120 kJ g^{-1}. The H_2 production rate at 0.5 A cm^{-2} is 2.59×10^{-6} mol H_2 cm^{-2} s^{-1}. H_2 power out = H_2 production rate × LHV = 0.625 W cm^{-2}. Efficiency = H_2 power out/Electrolyzer power × 100%= 52.08%. (ii) Electricity cost of hydrogen production. Mass of produced H_2 = H_2 production rate × Electrolyzer area × Molar mass H_2 × Time = 1.295 g H_2. Volume of H_2 = m/ρ = 1.295 g/ (0.09 g $liter^{-1}$) = 14.39 liters. Energy consumption = Electrolyzer power / (H_2 production rate × Molar mass H_2) = 91.8 kW h/kg H_2. Electricity cost (H_2/kg) = Energy consumption Electricity bill = 91.8 kW h/kg H_2 × $ 0.02/kW h = $ 1.836/kg H_2.

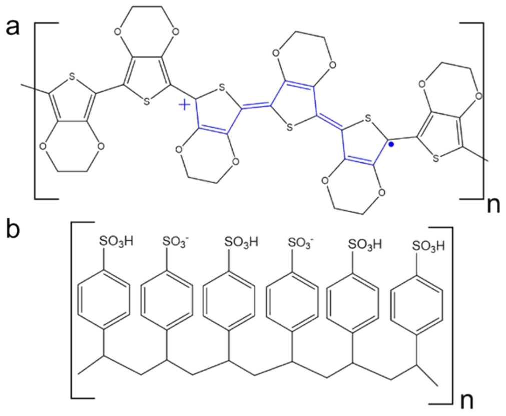

Fig. S1. Molecular structure of (a) PEDOT and (b) PSS.

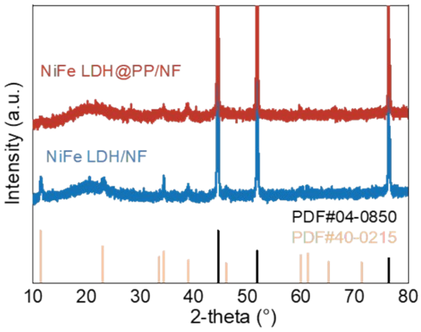

Fig. S2. XRD patterns of NiFe LDH/NF and NiFe LDH@PP/NF.

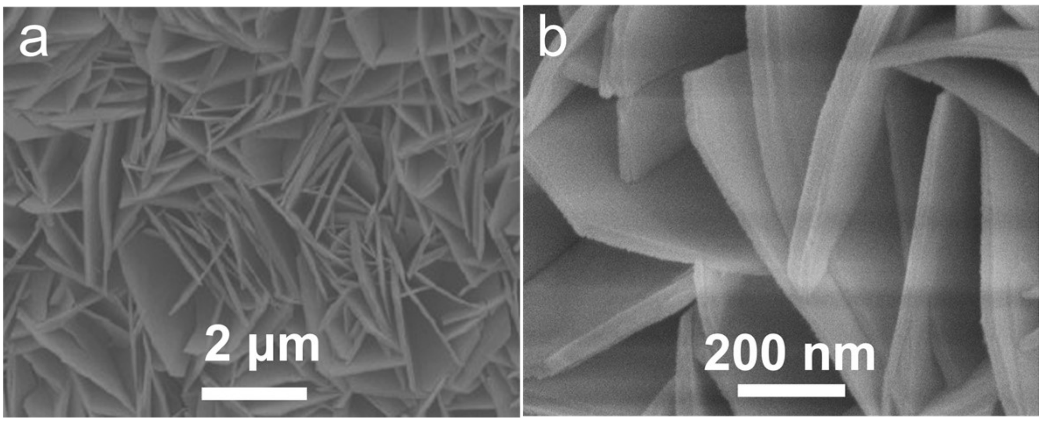

Fig. S3. (a) Low- and (b) high-magnification SEM images of NiFe LDH/NF.

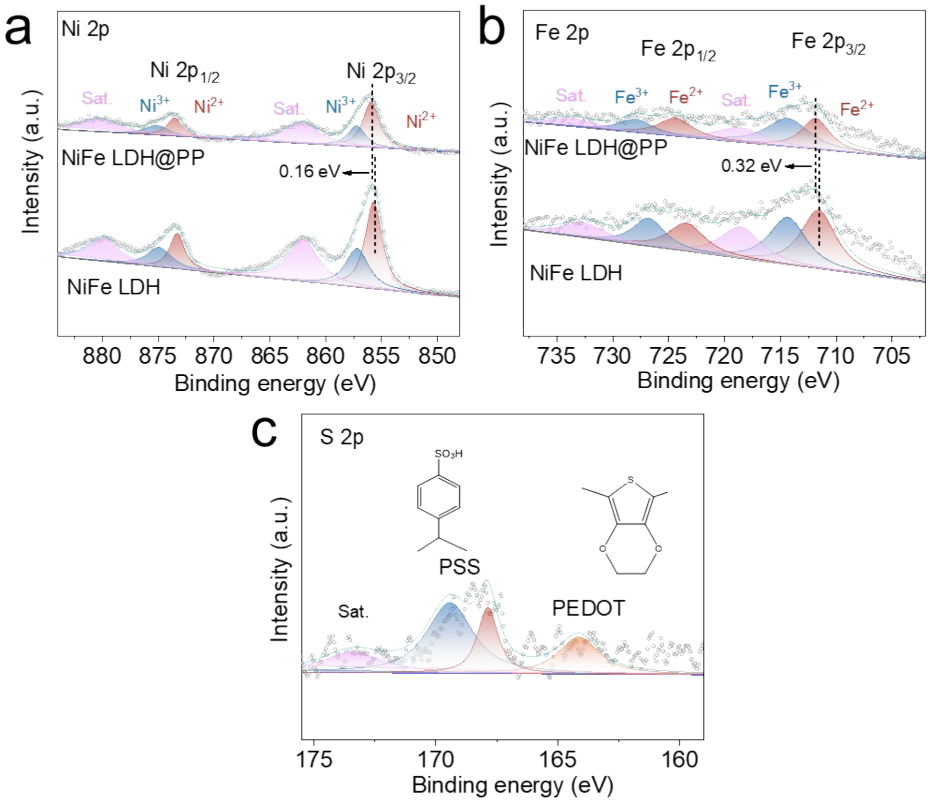

Fig. S4. High-resolution XPS spectra of NiFe LDH and NiFe LDH@PP in the (a) Ni 2p and (b) Fe 2p regions. (c) High-resolution XPS spectrum of NiFe LDH@PP in the S 2p region.

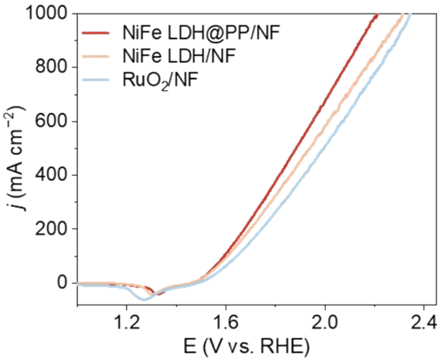

Fig. S5. LSV curves of different electrocatalysts in 1 M KOH + seawater without iR compensation.

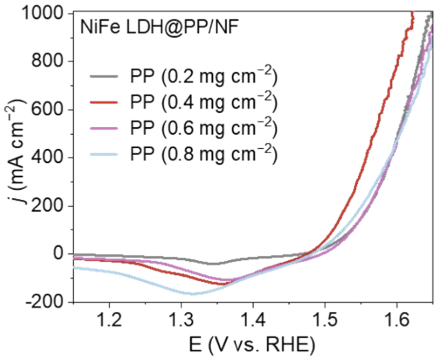

Fig. S6. LSV curves of NiFe LDH@PP/NF with different PP loading amounts in 1 M KOH + seawater.

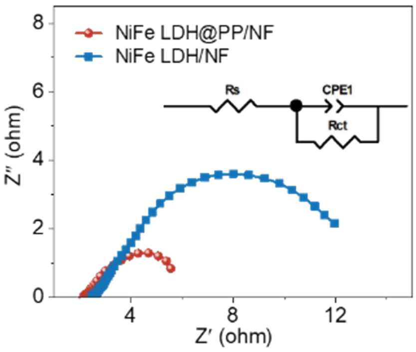

Fig. S7. Nyquist plots of NiFe LDH@PP/NF and NiFe LDH/NF in 1 M KOH + seawater.

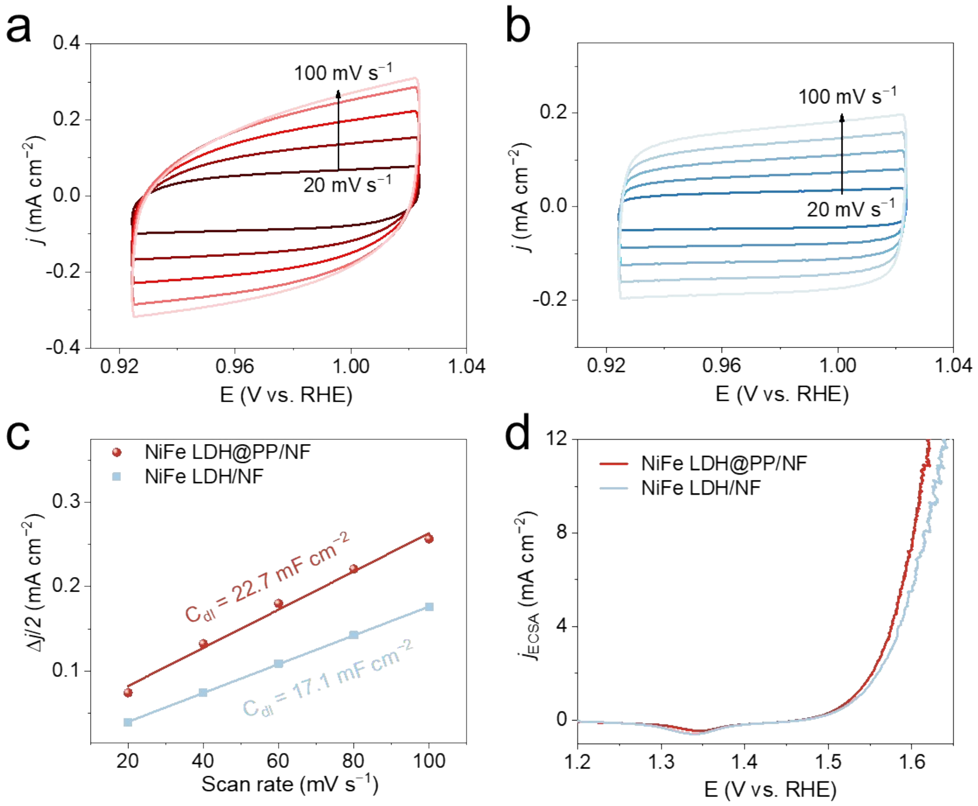

Fig. S8. CV curves of (a) NiFe LDH@PP/NF and (b) NiFe LDH/NF in the double layer region at different scan rates of 20 to 100 mV s^{-1} in 1 M KOH + seawater. (c) Electrochemical double-layer capacity of NiFe LDH@PP/NF and NiFe LDH/NF. (d) ECSA-normalized LSV curves of NiFe LDH@PP/NF and NiFe LDH/NF in 1 M KOH + seawater.

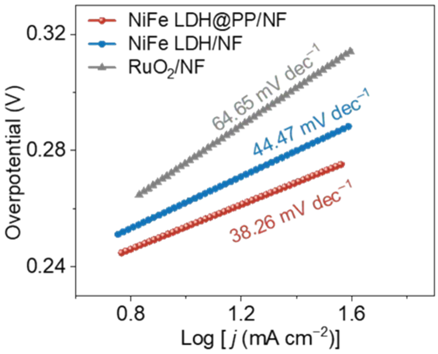

Fig. S9. Tafel plots of different electrocatalysts in 1 M KOH + seawater.

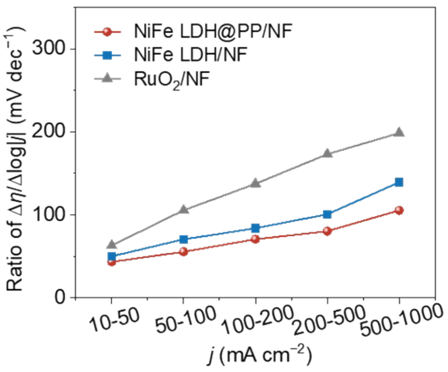

Fig. S10. $\Delta\eta/\Delta\log|j|$ ratios under a series of j intervals.

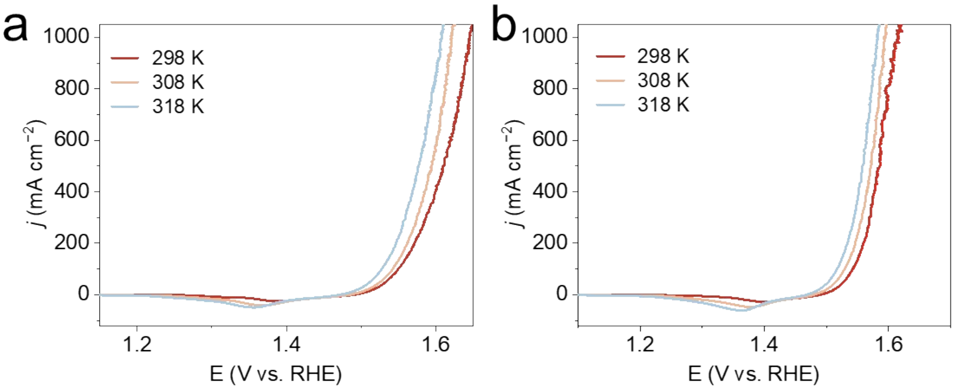

Fig. S11. LSV curves of (a) NiFe LDH/NF and (b) NiFe LDH@PP/NF at different temperatures in 1 M KOH + seawater.

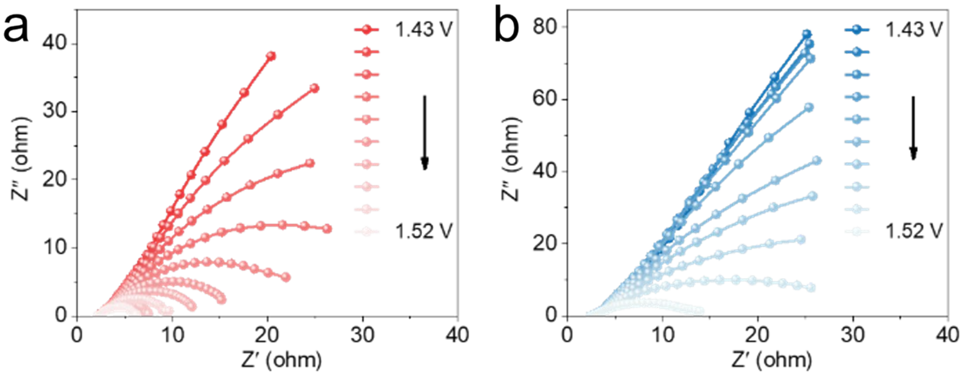

Fig. S12. Nyquist plots at various voltages of (a) NiFe LDH@PP/NF and (b) NiFe LDH/NF.

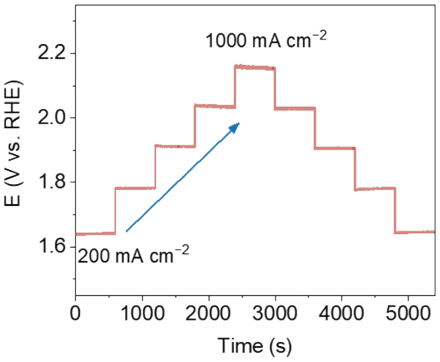

Fig. S13. Multistep chronopotentiometric curve of NiFe LDH@PP/NF without iR correction in 1 M KOH + seawater.

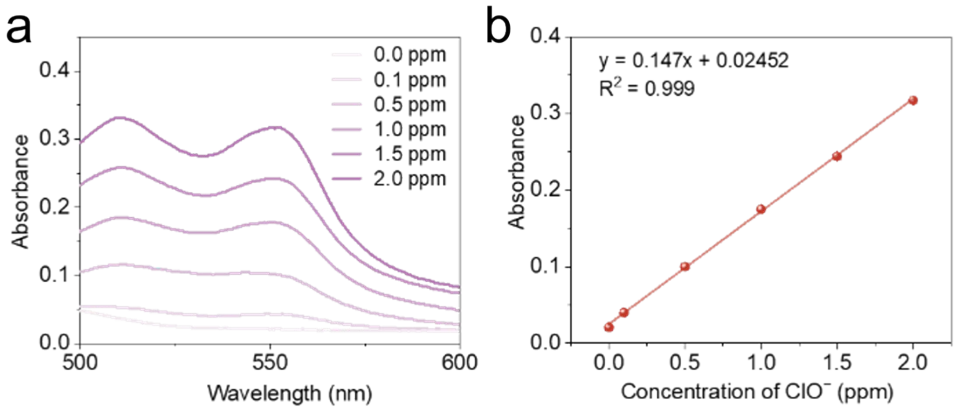

Fig. S14. (a) UV-vis absorption spectra of various active chlorine concentrations and (b) corresponding linear fit.

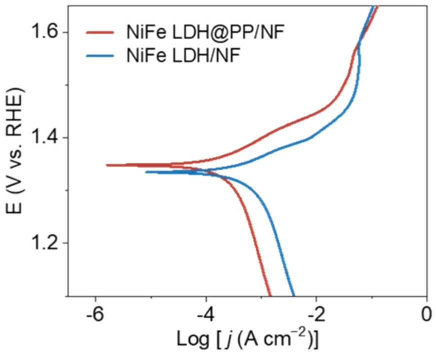

Fig. S15. Corrosion polarization plots of the NiFe LDH/NF and NiFe LDH@PP/NF in 1 M KOH + seawater.

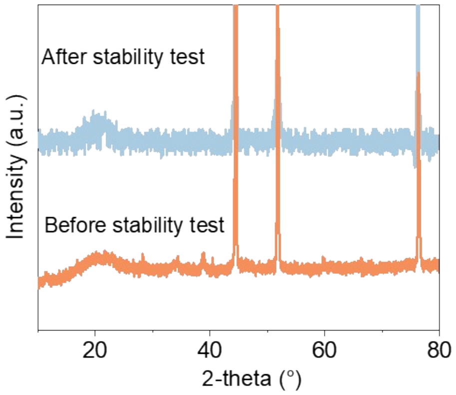

Fig. S16. XRD patterns of NiFe LDH/NF before and after 150-h stability test in 1 M KOH + seawater.

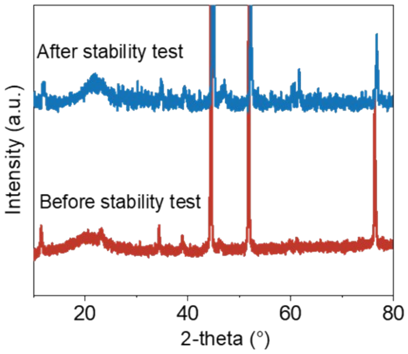

Fig. S17. XRD patterns of NiFe LDH@PP/NF before and after 800-h stability test in 1 M KOH + seawater.

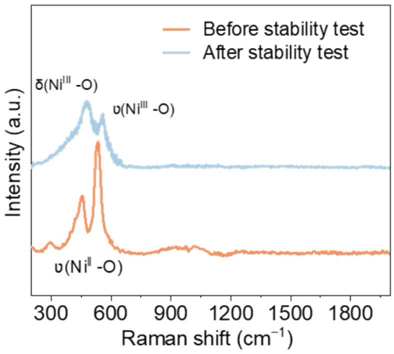

Fig. S18. Raman spectra of NiFe LDH/NF before and after 150-h stability test in 1 M KOH + seawater.

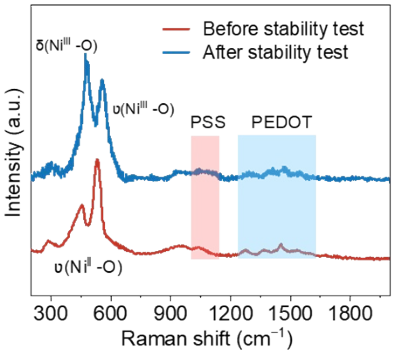

Fig. S19. Raman spectra of NiFe LDH@PP/NF before and after 800-h stability test in 1 M KOH + seawater.

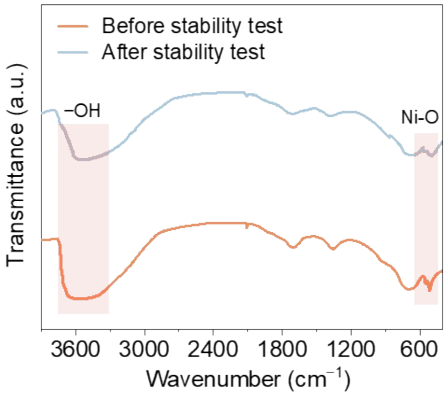

Fig. S20. FT-IR spectra of NiFe LDH/NF before and after 150-h stability test in 1 M KOH + seawater.

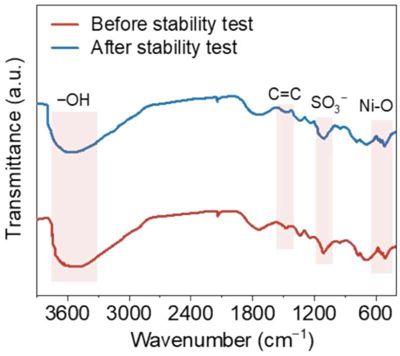

Fig. S21. FT-IR spectra of NiFe LDH@PP/NF before and after 800-h stability test in 1 M KOH + seawater.

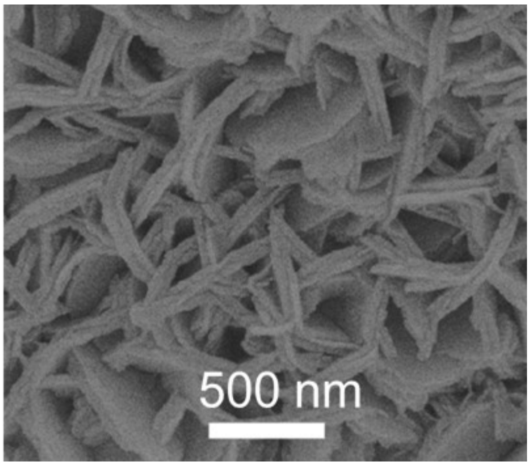

Fig. S22. SEM images of NiFe LDH@PP/NF after 800-h durability test in 1 M KOH + seawater.

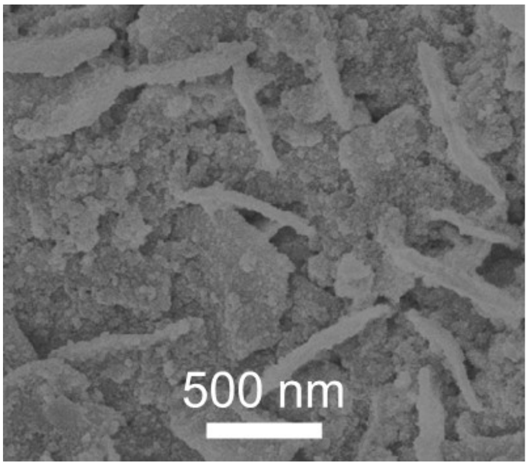

Fig. S23. SEM images of NiFe LDH/NF after 150-h durability test in 1 M KOH + seawater.

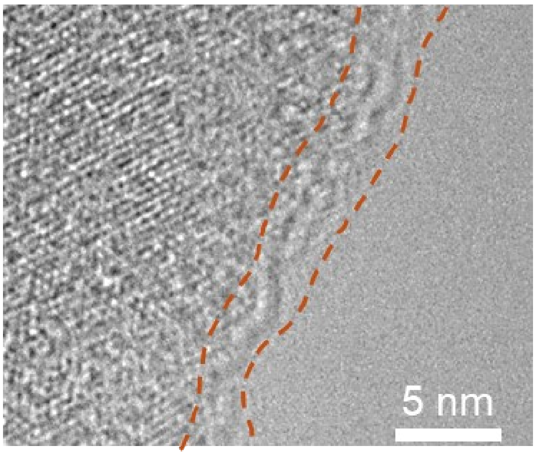

Fig. S24. HRTEM image of NiFe LDH@PP after 800-h durability test in 1 M KOH + seawater.

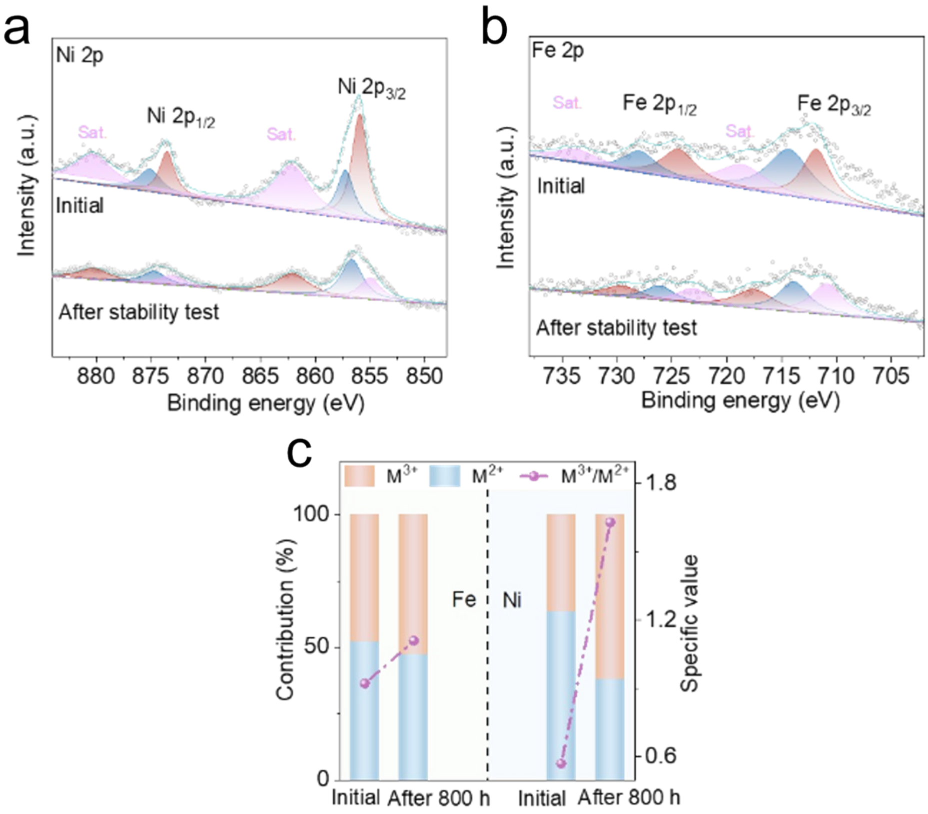

Fig. S25. High-resolution XPS spectra of NiFe LDH@PP in the (a) Ni 2p and (b) Fe 2p regions before and after 800-h durability test in 1 M KOH + seawater. (c) Changes of metal valence ratio before and after the test.

Table S1. Comparison of the OER performance of NiFe LDH@PP/NF with other reported electrocatalysts.

Catalysts	Current density (mA cm^{-2})	Overpotential (mV)	Ref.
NiFe LDH@PP/NF	**1000**	**390**	**This work**
S-Ni/Fe(OOH)/NF	1000	462	*Energy Environ. Sci.*, 2020, **13**, 3439
Ni_2P-Fe_2P/NF	1000	431	*Adv. Funct. Mater.*, 2021, **31**, 2006484
NiFeO-CeO_2/NF	1000	408	*ACS Nano*, 2023, **17**, 16008−16019
Fe-NiS/NF	1000	420	*Inorg. Chem.*, 2023, **62**, 7976−7981
TS-NiFe LDH	1000	412	*Small*, 2024, **20**, 2311431
S-(Ni,Fe)OOH/NF	500	398	*Energy Environ. Sci.*, 2020, **13**, 3439
$MnCo_2O_4$@NiFe LDH/NF	500	578	*J. Colloid Interface Sci.*, 2023, **632**, 54−64
BZ-NiFe-LDH/CC	500	610	*Nano Res. Energy*, 2022, **1**, e9120028
NiMoN@NiFeN	1000	398	*Nat. Commun.*, 2019, **10**, 5106
NiFeMOF@ $Ni_2P/Ni(OH)_2$	1000	394	*J. Colloid Interface Sci.*, 2023, **643**, 17–25
NiFe-LDH-6-4/CC	100	301	*Mater. Today Energy*, 2021, **22**, 100883
RuMoNi	1000	470	*Nat. Commun.*, 2023, **14**, 3607
Ru-FeP_4/NF	1000	520	*Appl. Catal. B: Environ.*, 2022, **319**, 121950
RuNi-Fe_2O_3	1000	497	*Chin. J. Catal.*, 2022, **43**, 2202–2211.

Table S2. The stability of NiFe LDH@PP/NF compared with some recently reported electrodes in alkaline seawater.

Catalysts	**Current density (mA cm^{-2})**	**Time (h)**	**Ref.**
NiFe LDH@PP/NF	**1000**	**800**	**This work**
BZ-NiFe-LDH	500	100	*Nano Res. Energy*, 2022, **1**,
NiPO$_x$@NiFe LDH/NF	1000	600	*J. Colloid Interface Sci.*, 2025, **687**, 708–714
NiFe LDH@PTPA/NF	1000	600	*ACS Mater. Lett.*, 2024, **6**,
NiCoP foam	1000	300	*J. Mater. Chem. A*, 2024, **12**, 2680−2684
NiMoS$_x$@NiFe-LDH	500	500	*Inorg. Chem. Front.*, 2023, **10**, 2766–2775
Cr-Co$_x$P/NF	100	140	*Adv. Funct. Mater.*, 2023, **33**, 2214081
NiFe LDH-CeW@NFF	1000	100	*Appl. Catal. B: Environ.*, 2023, **330**, 122612
NiFeS/NF	500	24	*J. Mater. Chem. A*, 2023, **11**, 1116–1122
Fe-NiSOH/NF	500	900	*Energy Environ. Sci.*, 2022, **15**, 4647
S-Ni/Fe(OOH)/NF	100	100	*Energy Environ. Sci.*, 2020, **13**, 3439
MnCo/NiSe/NF	500	200	*Appl. Catal. B: Environ.*, 2023, **325**, 122355
Ni_3S_2/Fe-NiP$_x$/NF	1000	225	*Adv. Sci.*, 2022, **9**, 2104846
NiIr-LDH	500	650	*J. Am. Chem. Soc.*, 2022, **144**, 9254–9263
60Fe	250	100	*Adv. Energy Mater.*, 2023, **13**, 2301921
NiS@LDH	200	100	*Small*, 2023, **19**, 2300194
$Fe_2P/Ni_{1.5}Co_{1.5}N/Ni_2P$	100	40	*ACS Nano*, 2023, **17**, 1681−1692
NiCoS	100	100	*Appl. Catal. B: Environ.*, 2021, **291**, 120071
Fe_2O_3/NiO	100	50	*ACS Appl. Mater. Interfaces*, 2021, **13**, 37152–37161

Table S3. Element concentrations of electrolytes for NiFe LDH@PP/NF and NiFe LDH/NF after stability test.

	Element	**Element concentration (mg/L)**
NiFe LDH/NF	Ni	1.864
	Fe	0.357
NiFe LDH@PP/NF	Ni	0.089
	Fe	0.057